AIAA 80-0769R

Recent Development of the YF-17 Active Flutter Suppression System

C. Hwang,* E.H. Johnson,† and W.S. Pi†
Northrop Corporation, Hawthorne, Calif.

Active wing/store flutter suppression systems were demonstrated in 1977 in a series of wind tunnel tests on a YF-17 scale model. In order to substantially improve the suppression system performance, new control laws were developed based on multiple feedback loops, multiple control surfaces, or both. For test safety, a flutter sensing unit and a new store, functioning as a flutter stopper, were designed and fabricated. Test monitoring programs were organized on a Hewlett-Packard 5451C Fourier Analyzer that permitted a real time assessment of the control law effectiveness. One of the monitoring programs generated the aircraft open loop transfer function and Nyquist plots in the supercritical region while the flutter suppression loop was closed. In the tests performed in late 1979, the new control laws were applied to suppress a severe flutter condition to 70% above the uncontrolled flutter dynamic pressure. Postanalysis of the test data indicated the potential to increase the dynamic pressure to an even higher level.

Nomenclature

a	= constants used in the pseudo-integrator $1/(s+a)$
$a_1,\ldots,a_4$	= accelerometer outputs (g)
c,c'	= damping coefficients
c_0	= critical damping coefficient
$F_1,\ldots,F_4$	= pseudo integrators (Fig. 2)
$\bar{F}_1,\ldots,\bar{F}_4$	= feedback loop transfer functions (Fig. 4)
G,G_1,G_2,G_A	= transfer functions of aircraft model response and the servo-actuator system
G_{ij}	= open loop transfer functions of aircraft model response (i) due to control servo input (j)
$G_{ij,c}$	= corresponding closed loop transfer functions of G_{ij}
M	= Mach number
Q	= dynamic pressure (psf)
Q_f	= flutter dynamic pressure (psf)
$R_1,\ldots,R_5$	= potentiometer settings
s	= Laplace operator
α	= typical transducer signal
$\delta_c,\delta_{\text{IN,LE}}$ $\delta_{\text{IN,TE}}$	= inputs to leading edge or trailing edge surface servos
η_1,η_2	= responses to noise
θ_{01},θ_{02}	= model responses
ω,ω_n	= frequency and natural frequency (rad/s)

Introduction

WING/STORE flutter has been a significant factor in degrading the speed performance of combat aircraft. In the past decade, analytical and experimental work on active wing/store flutter suppression has produced promising results and demonstrated its potential for providing significant improvements in aircraft operational and mission effectiveness. Since active flutter suppression systems can use electro-hydraulic feedback networks to counteract the flutter conditions, the eventual integration of the suppression system into an advanced aircraft control system holds promise of extending the aircraft performance with a minimal increase in control hardware.

In order to develop a working suppression system dealing with wing/store flutter and to resolve technical problems in actual systems implementation, an active flutter suppression system was designed and incorporated into a 30% scale model of the YF-17 aircraft. The model has a leading edge and a trailing edge control surface. A store configuration was intentionally designed that featured a violent flutter condition. In the series of wind tunnel tests performed in 1977, a feedback control system, consisting of a number of filters and a simple gain, phase shift circuit was able to suppress the violent flutter condition. For instance, at $M=0.60$, the projected improvement in the flutter dynamic pressure was 29%. The analytical and test results related to the test sequence are documented in Refs. 1 and 2.

The experience gained in the above-mentioned wind tunnel tests pointed the way to further improvements that could be made in the flutter suppression system and the supporting hardware. A new test sequence was initiated and conducted with the objectives of 1) augmenting and upgrading the mechanical and electrical components, 2) designing more complex control laws with the goal of a demonstrated improvement of 70% in the flutter dynamic pressure, and 3) using the Hewlett-Packard 5451C Fourier Analyzer to monitor the control law performance and to point out ways the laws could be improved.

In order to concentrate the new test effort on flutter control law development and suppression system performance, a single test configuration was selected which featured the above-mentioned severe flutter condition. Prior to test entry, a number of control laws were developed using either one or two control surfaces and reflecting different control philosophies. These control laws were mechanized and integrated into the flutter suppression electronics console at Northrop's Hawthorne facility.

The wind tunnel tests were performed in Sept.-Oct. 1979 at the NASA Langley Center 16-ft Transonic Dynamics Tunnel. This paper describes briefly the major features of the improved YF-17 flutter suppression model, the test monotoring techniques, and the analytical and experimental results of the newly-developed control laws.

Received March 7, 1980; presented as Paper 80-0769 at the AIAA/ASME/ASCE/AHS 21st Structures, Structural Dynamics and Materials Conference, Seattle, Wash., May 12-14, 1980; revision received Oct. 31, 1980.

*Manager, Structural Dynamics Research, Aircraft Division. Associate Fellow AIAA.

†Engineering Specialist, Structural Dynamics Research, Aircraft Division. Member AIAA.

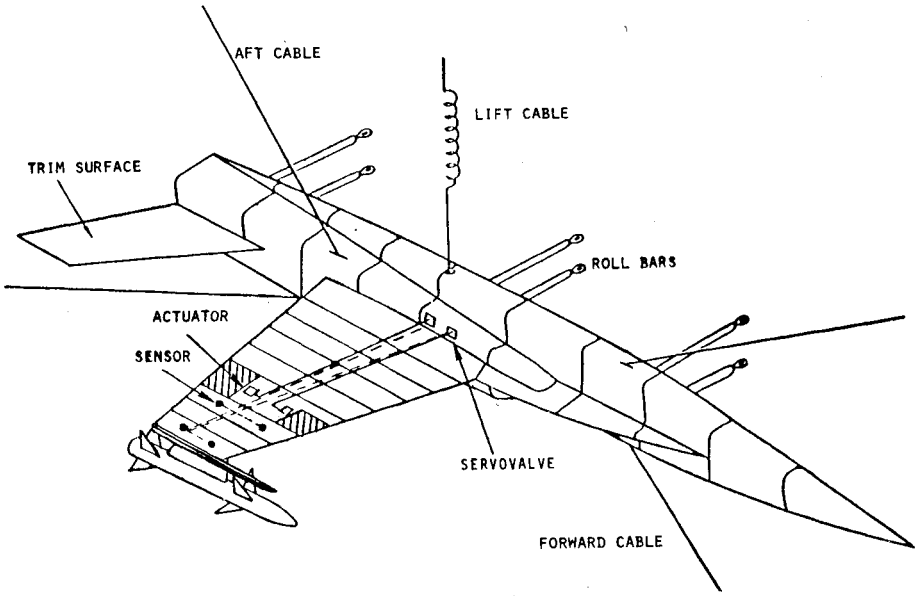

Fig. 1 YF-17 wing/store flutter suppression model, Configuration B.

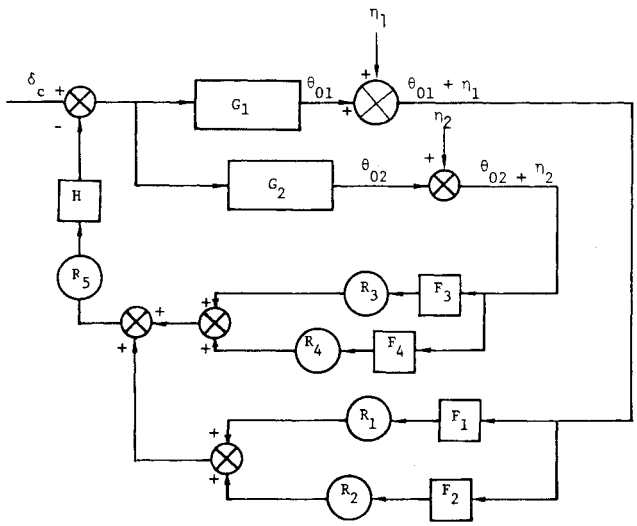

Fig. 2 Representative block diagram for a control law used during the tunnel test.

The Improved Model and New Instrumentation Features

The YF-17 flutter suppression model is a 30% scale half span model mounted on a set of roll bars and stabilized with forward and aft tension cables. Leading edge and trailing edge control surfaces are operated by miniaturized hydraulic actuators. A detailed arrangement of the model in its test configuration is shown in Fig. 1.

The basic test configuration adopted is called Configuration B. It features an empty tip launcher rail and an AIM-7S missile attached to a pylon near the wing tip (W.S. 60.75). As part of the refurbishing work, the leading edge and trailing edge surface hinge mechanisms were completely redesigned to improve their ruggedness. The original angular potentiometers attached to the hinges were replaced with rotary variable differential transformers (RVDT's). It also featured new surface-to-actuator shaft-attachments for improved reliability and interchangeability.

Four Sundstrand accelerometers were installed in the wing sections to serve as the main transducers for flutter suppression. The transducers, identified as a_1 through a_4, were installed in the following locations:

Accelerometer No. 1 (a_1) W.S. 51.45
F.S. 145.18 (25%c)

Table 1 Control laws for the YF-17 flutter suppression model

Control law	Control surface Leading edge	Control surface Trailing edge	Accelerometers a_1	a_2	a_3	a_4
N1	X				X	X
N3	X		X		X	X
N3T		X	X		X	X
N3P	X	X	X		X	X

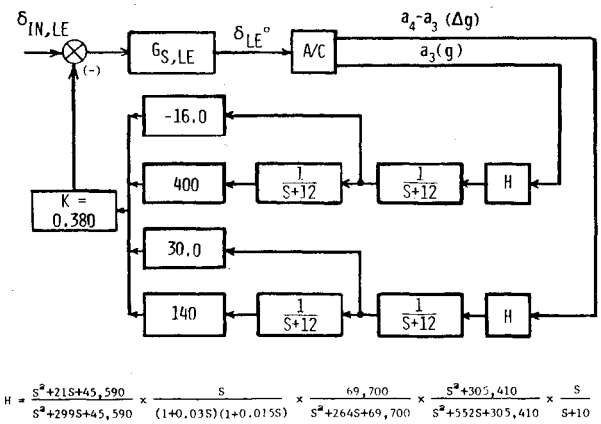

Fig. 3 The leading edge surface control law (N1).

Accelerometer No. 2 (a_2) W.S. 51.45
F.S. 158.00 (76%c)

Accelerometer No. 3 (a_3) W.S. 60.75
F.S. 148.56 (25%c)

Accelerometer No. 4 (a_4) W.S. 60.75
F.S. 157. 47 (70%c)

Control Law Definition and Analysis

Detailed open loop flutter analyses were performed on the YF-17 model. The results were correlated with previous wind tunnel test data of the same model (Refs. 1 and 2). Once confidence in the open loop analysis had been attained, the construction of new control laws could proceed. Figure 2 is a representative block diagram of the new control laws. In the figure, θ_{01} and θ_{02} are two model response outputs (e.g., the angular and vertical accelerations derived from the outboard sensor pair) which are filtered, blended, and then fed back to

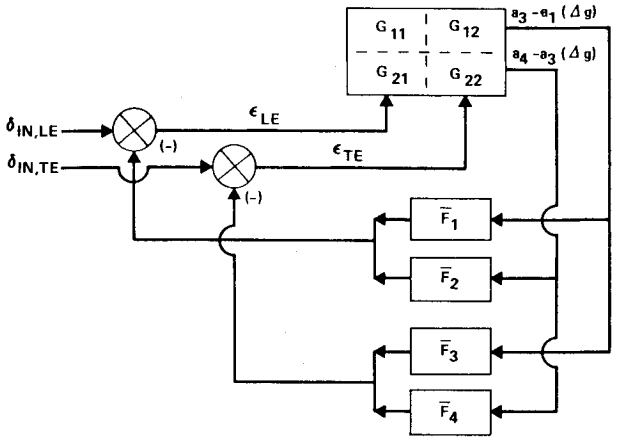

Fig. 4 The two-surface control law (N3P).

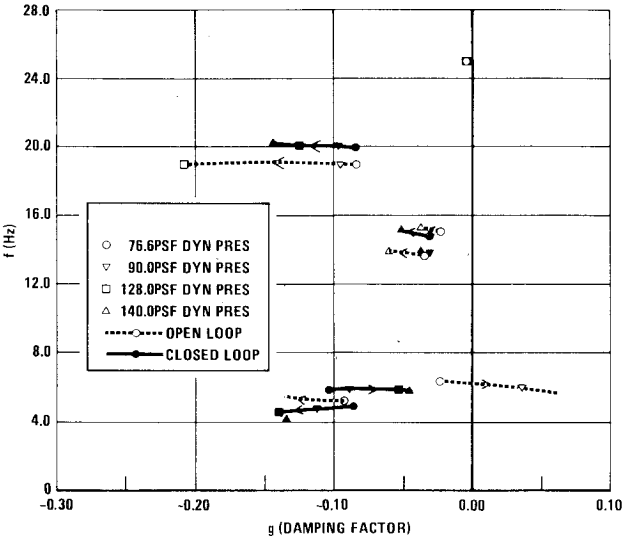

Fig. 5 Characteristic diagram results of the YF-17 model with and without the leading edge surface control law (N1), $K=0.75$.

one of the control surfaces. The F_i terms are pseudo-integrators which convert the accelerometer outputs to responses which approximate velocity and displacement signals. The "pseudo" designation is used because the integrators are of the form $1/(s+a)$ with the a used to prevent steady state drift. The R_i components are gain settings which control the combination of the velocity and displacement signals, with the R_5 term controlling the overall gain.

A synthesis procedure[3] was applied to determine the constants R_1 through R_4. Altogether, four control laws were organized by Northrop and tested in the wind tunnel. They are identified as control laws N1, N3, N3T, and N3P. The control surfaces and the accelerometers used by each of these control laws are identified in Table 1. Specifically (N1) and (N3) are leading edge control laws. (N3T) is a trailing edge control law. (N3P) uses both the leading edge and trailing edge control surfaces and is a superposition of control laws (N3) and (N3T). The block diagrams of Northrop control laws (N1), (N3P) are shown in Figs. 3 and 4.

Pretest analyses were performed on all control laws, with some additional analyses made at Hawthorne while the test was in progress at the NASA Langley TDT facility. Figure 5 is a plot of the stability behavior of the open loop system and of control law (N1) at $M=0.80$ using dynamic pressure Q as a parameter. The data were acquired by the characteristic diagram method.

Test Monitoring Techniques

An important aspect of the project was the development of procedures that monitor and direct the wind tunnel test program. Prior to the test entry, monitoring programs were developed on the Hewlett-Packard 5451C Fourier Analyzer. Actual servo hardware and an analog simulation of the YF-17 model were used to try out and debug the monitoring programs. In this section, some key monitoring programs used in the tunnel entry are described.

Nyquist Plot

A key monitoring program was developed to extract the open loop transfer function of the YF-17 flutter suppression system when the control loop was closed. If G_A and G are the transfer functions of the actuator/servo and the aircraft, and H is the transfer function of the feedback loop, then the closed loop transfer function of the complete system is:

$$G_c = \frac{G_A G}{1+G_A GH} \tag{1}$$

The Nyquist criterion requires a plot of $G_A GH$. The assumption for developing the test monitoring technique was that it should be possible to make a relatively accurate measurement of G_c but that a direct measurement of G would be difficult since it would require the measurement of a mode that was suppressed and because noise would contaminate a measurement made inside the loop. The alternative was to extract G from the measured values of G_c, G_A, and H. (The latter two transfer functions could be and were measured very well with the loop open, and were then stored on a computer disk.) The open loop transfer function was then obtained from Eq. (1):

$$G = \frac{G_c}{G_A(1-G_cH)} \tag{2}$$

The application of the Nyquist plot technique in actual wind tunnel test will be illustrated later in the section dealing with experimental results.

The measurement of the closed loop transfer functions required that some type of excitation be applied at the servo-input junction, such as the δ_c point of Fig. 2. During the simulation work carried out at Hawthorne, as well as during the later wind tunnel test, the excitation utilized was a random transient that was generated by the Fourier Analyzer. This was a random noise signal that was set to zero in the last 25% of the sample period. This made the response to the excitation die out in the sample period (i.e., it was periodic in the "window") and Fast Fourier Transform techniques were valid.

Smoothing of Transfer Functions

Another test monitoring program dealt with the smoothing of frequency domain signals such as aircraft transfer functions. Because of the substantial level of turbulence in the tunnel, the response signal to noise ratios were such that key modal information was masked by the superimposed noise. In order to reduce the noise effect, smoothing techniques were applied to the measured transfer functions. Methods of smoothing entail performing a Fourier transform on the transfer function to obtain the impulse response of the system. It is assumed that all the response after a certain time in this record is uncorrelated with the input excitation. A simple means of removing this response is to apply a rectangular window to the impulse response that zeroes out all response after a certain time. When this truncated response is transformed back to the frequency domain, the resulting transfer function is considerably cleaner, but retains all the key modal information.

Peak-Hold Damping Trend

The peak-hold spectrum method provides frequency domain measurements of the model responses, filtered through 250 narrow-band circuits. The peak response within each interval is registered on a screen until the peak amplitudes are stabilized. The damping of a resonant mode is assumed to be proportional to the inverse of the peak amplitude. The damping trend data can be extrapolated readily during the test along the dynamic pressure Q to determine the projected flutter point for the flutter suppression system. The method was used extensively in the tunnel test to determine the control system effectiveness and, with the assistance of other monitoring programs, to revise the tunnel test strategy.

Experimental Results

Peak-Hold Damping Data

After setting up the YF-17 flutter suppression model in the NASA Langley TDT facility and performing a simple ground vibration test, actual wind-on tests were initiated in early October. Altogether, 27 runs were made consisting of 511 test points. The key results for the uncontrolled flutter model and for the model with control laws (N1) and (N3P) are summarized in Figs. 6-8 in the form of peak-hold damping trend plots. The plots were based on the signals from the wing torsion moment gage.

A review of the damping trends for the open and closed loop cases clearly demonstrated the effectiveness of the flutter suppression system. The data also indicate that, compared to control law (N3P), control law (N1) has a larger margin in the extrapolated dynamic pressure range, even though the surface activity data indicate the two surface law (N3P) is a more effective control law. This point will be discussed further in the following subsection dealing with rms response data.

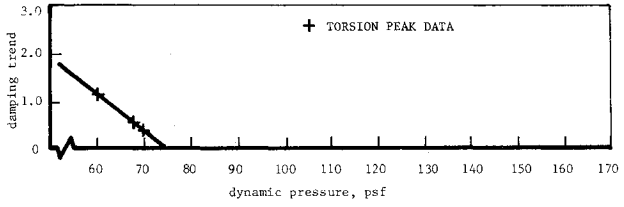

Fig. 6 Damping trend of the YF-17 flutter suppression model—open loop, $M = 0.80$.

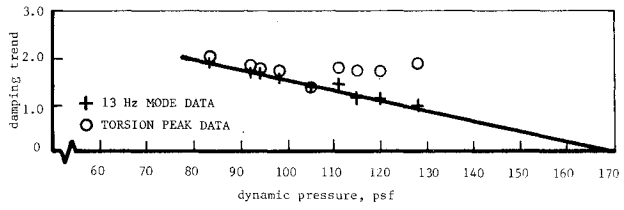

Fig. 7 Damping trend of the Northrop leading edge surface control law (N1) (Test Point 89-103).

Rms Response Data

The FM tape data were processed to calculate power spectrum information for the majority of the test points where peak hold information was taken. The purpose of this analysis was to provide a more quantitative comparison of the various control laws. It also provided insight into the model behavior and into the subjective criteria that were used to guide the conduct of the test.

Table 2 presents rms values for the control surface and the two strain gage bridges that were mounted on the wing root. The results are presented in two frequency ranges, allowing for the distinction between the lower frequency response associated with the open loop flutter mode and those associated with the higher frequencies. The first line in Table 2 gives the responses at the highest open loop dynamic pressure at which the model was tested for comparison purposes. A careful examination of the data in this table

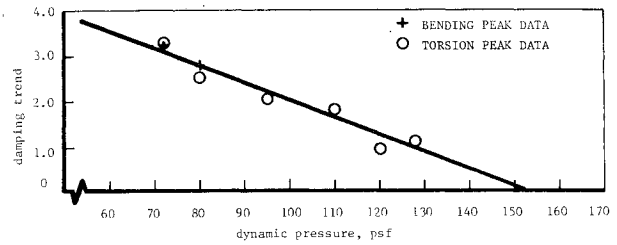

Fig. 8 Damping trend of the Northrop two-surface control law (N3P) (Test Point 487-508).

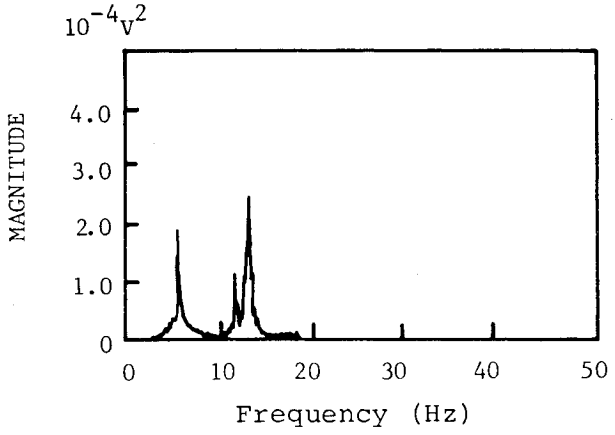

Fig. 9 The PSD of the leading edge surface angular displacement acquired at test point 104, $Q = 128$ psf, control law (N1).

Table 2 Rms response data of the YF-17 model for various control laws and at different dynamic pressures

Control law	Q psf	Test point	Control surface displacement (deg)		Wing bending moment (in.-lb)		Wing torsion moment (in.-lb)	
			0-10Hz	0-20 Hz	0-10 Hz	0-20 Hz	0-10 Hz	0-20 Hz
None	73	64	—	—	41.4	49.8	42.7	44.1
N3T	96	249	0.32	0.34	28.2	39.0	26.2	29.8
N1	98	97	0.52	0.86	29.9	51.0	8.3	22.1
N3	101	124	0.63	0.69	37.6	50.2	11.7	17.7
N1	128	104	0.70	1.10	41.7	61.0	9.0	28.6
N3	128	127	0.87	0.97	49.5	66.2	12.5	22.1
N3P[a]	128	510	0.52	0.66	42.0	59.0	18.0	26.9

[a] The control surface displacement rms data of control law (N3P) are for the leading edge surface.

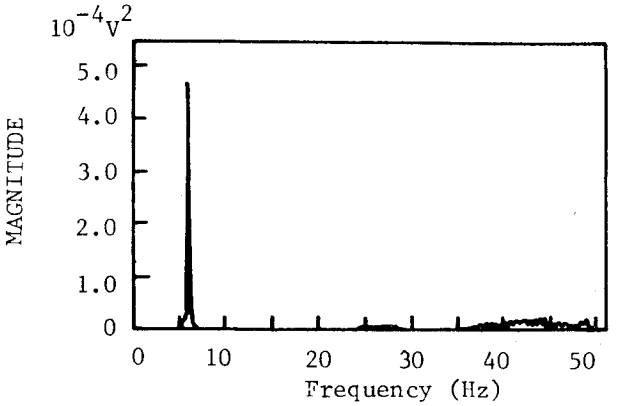

Fig. 10 The PSD of the wing root torsion gage output acquired at Test Point 64, open loop, $Q = 73$ psf.

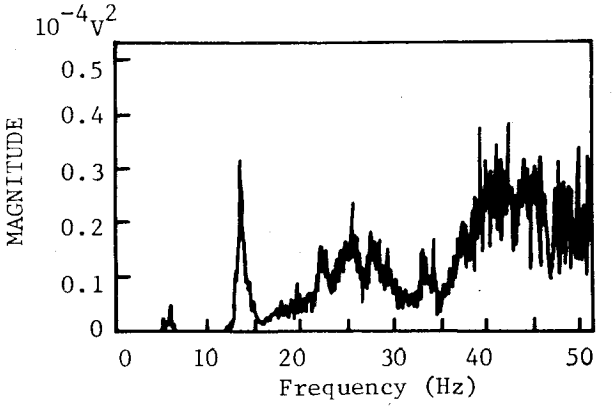

Fig. 11 The PSD of the wing root torsion gage output acquired at Test Point 104, $Q = 128$ psf, control law (N1).

reveals some of the subtleties of the various control laws. For instance, it is seen that the (N1) control law did a better job of suppressing the flutter mode than the N3 law, but that the N3 law had considerably less response in the 10-20 Hz range than the (N1) law. Figure 9 gives the power spectral response of the leading edge surface position for control law (N1), which shows substantial mode peaks in the 10-20 Hz range.

Another point from Table 2 is that the open loop response of Test Point 64 is quite high and, in fact, indicates that this was not a prudent condition at which to be testing. Figures 10 and 11 compare the PSD's of the wing torsion gage for the uncontrolled case of Test Point 64 with the controlled case at a dynamic pressure that is 75% higher. Note that there is 20 dB magnitude difference in the scales of the two figures. The uncontrolled PSD is dominated by the response at 6 Hz, while for the controlled case, the 6 Hz mode is suppressed so well that higher frequency modes dominate the response.

Table 2 also shows rms data for the trailing edge control law (N3T), and the (N3P) law, which used both control surfaces. The trailing edge law is seen to have required less control activity, but was not able to demonstrate as much of an improvement in dynamic pressure as the leading edge laws. Transfer function data tend to indicate that the trailing edge laws were characterized by low phase margins, making them sensitive to small changes in the feedback law or the tunnel condition.

The (N3P) control law performed well, particularly when it is considered that no attempt was made to improve upon the law during the tunnel test. The leading edge rms response is seen to be considerably less for the (N3P) law than for any of the single surface laws at an equivalent test condition. When the (N3P) law control surface PSD (not shown) was compared with the (N1) law data of Fig. 9, it was noted that the peak amplitudes were much less for the (N3P) law, although there

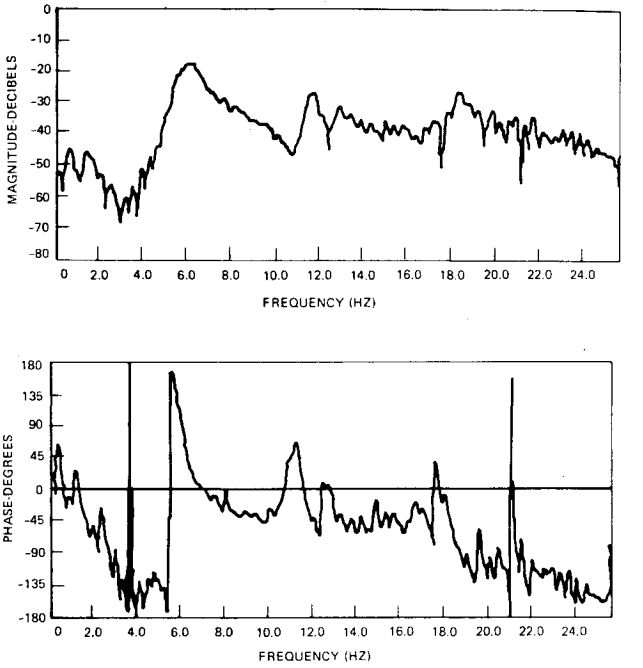

Fig. 12 Smoothed closed loop transfer function $(a_4 - a_3)$ vs $\delta_{IN,LE}$ acquired at Test Point 504, $M = 0.8$, $Q = 95$ psf, control law (N3).

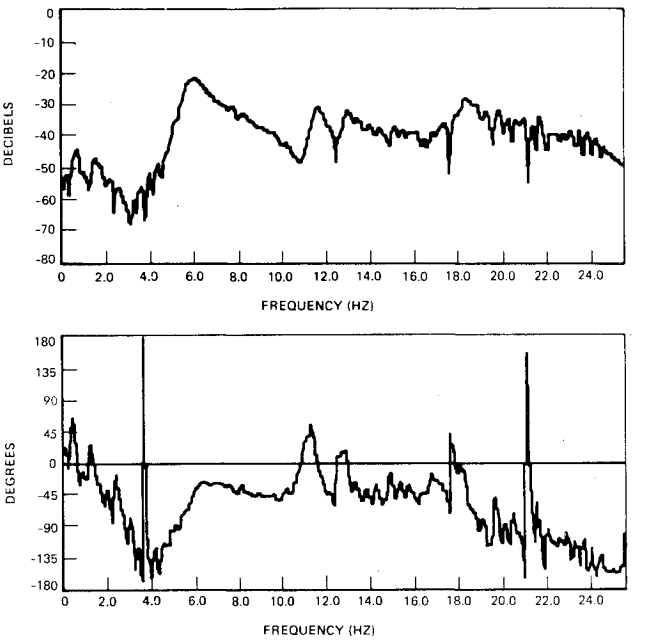

Fig. 13 Extracted open transfer function $(a_4 - a_3)$ vs the leading edge control surface input $\delta_{IN,LE}$, $M = 0.8$, $Q = 95$ psf.

was response over a broader frequency range. Unfortunately, trailing edge data were not recorded onto FM tape for the (N3P) law, but the impression formed during the test was that the trailing edge amplitude was less during the test of the (N3P) law than it was for the (N3T) law.

Closed Loop Transfer Function and Extraction of Open Loop Responses

During the wind tunnel tests, model transfer functions were acquired through control surface excitation. The excitation and measurement technique is described previously in the paper. The transfer functions generated onsite were used to monitor the model behavior and, for a closed loop system, to determine the effectiveness of the control law. Additional transfer functions were generated at Hawthorne based on the FM data and are called the postprocessed transfer functions.

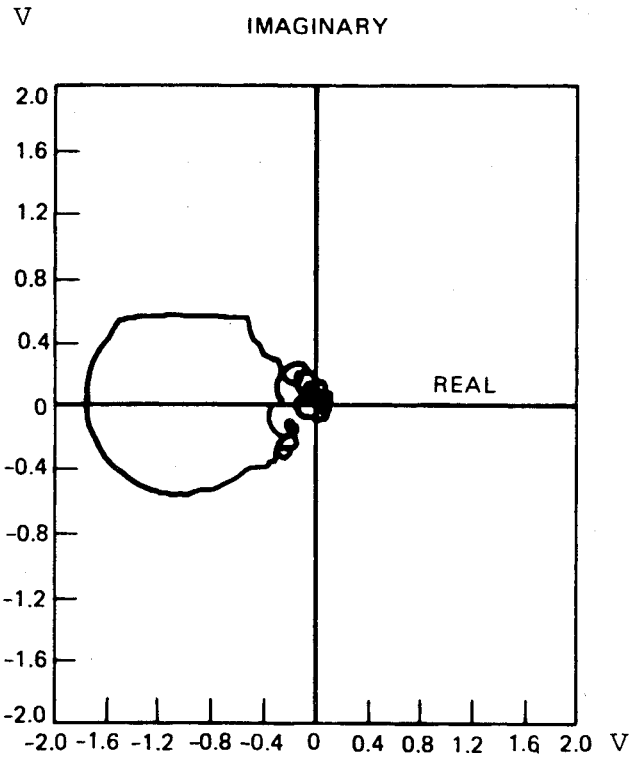

Fig. 14 Open loop Nyquist plot for the example presented in Figs. 12 and 13. The test condition was $M=0.8$, $Q=95$ psf, which is 27% above the critical open loop flutter dynamic pressure.

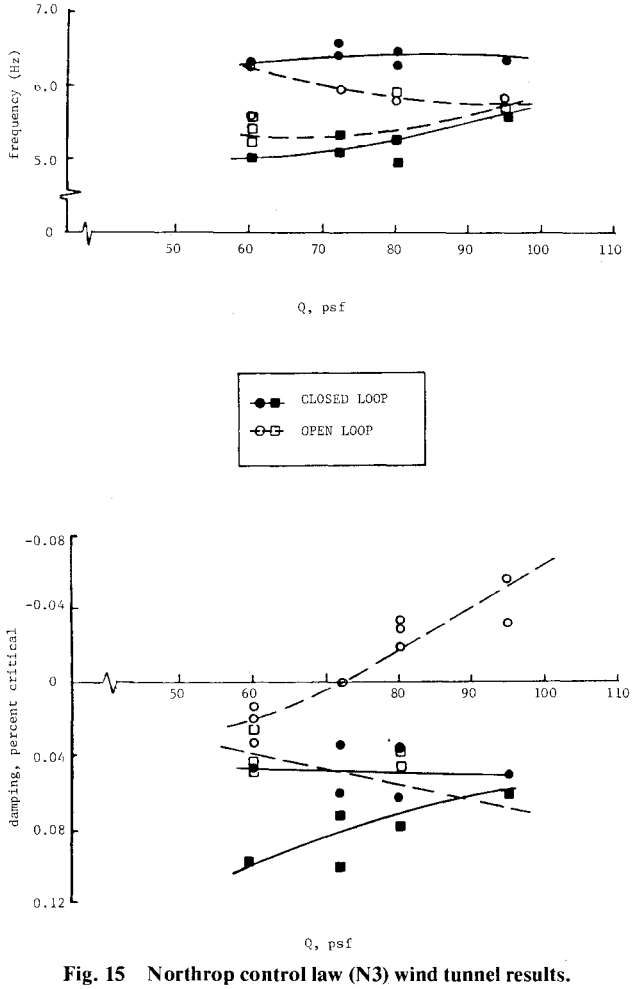

Fig. 15 Northrop control law (N3) wind tunnel results.

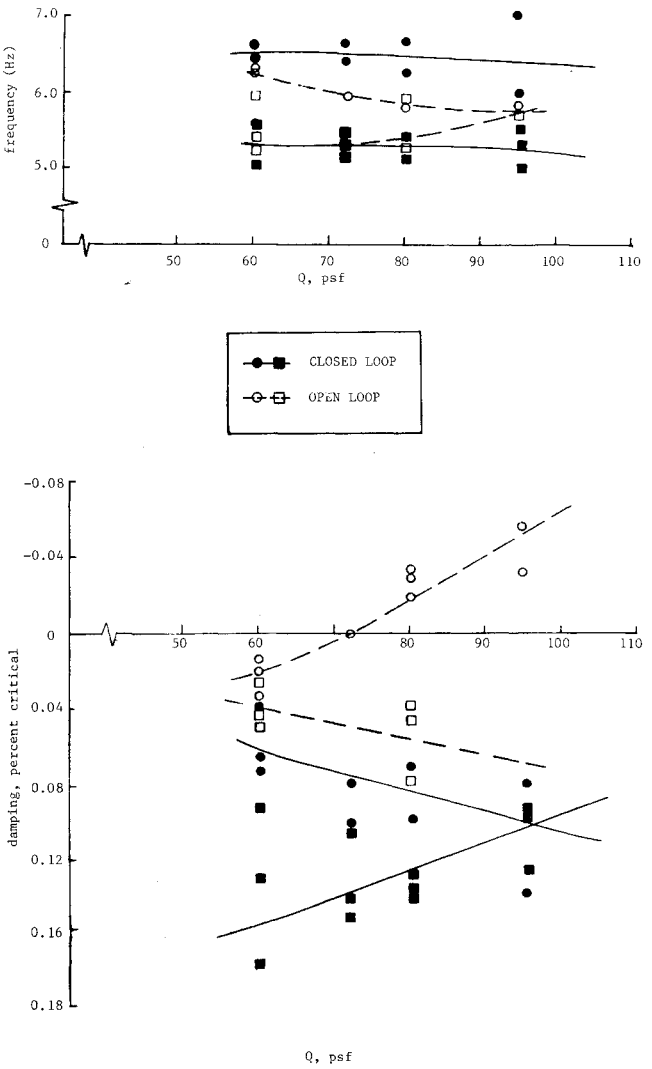

Fig. 16 Northrop leading and trailing edge control law (N3P) wind tunnel results.

Closed loop transfer functions were acquired for Test Point 504 at $M=0.80$, $Q=95$ psf, with control law (N3) in force. After smoothing, the result of (a_4-a_3) vs $\delta_{IN,LE}$ is given in Fig. 12. The transfer function (a_3-a_1) vs $\delta_{IN,LE}$ data were also acquired but are not shown here. In order to extract the open loop transfer functions for Nyquist criteria analysis, it is necessary to establish the feedback functions $F_iH(i=1,4)$ as shown in the block diagram of Fig. 2. These data were generated and stored, while the R_i parameters for the test point under consideration were, respectively, 0.365, 0.116, 0.351, 0.837 and 0.750. Figure 13 shows the open loop transfer function for (a_4-a_3), based on Eq. (2), and the measured closed loop and feedback component transfer function data.

With the open loop transfer functions, it is possible to construct the open loop Nyquist plot from which, for the case of a single control surface, the system gain and phase margins can be readily determined. The Nyquist function is the transfer function of the feedback signal vs the actuator input when the feedback junction is open. For the case of Test Point 504, described above, the resulting Nyquist plot is shown in Fig. 14. It is seen that the plot has the desirable encirclement around the -1 point, indicating control law (N3) at this test condition has large gain and phase margins.

During the wind tunnel test, a number of Nyquist plots were acquired in the above described manner. They were valuable in determining the margins of the control system, as well as in defining ways of improving control laws.

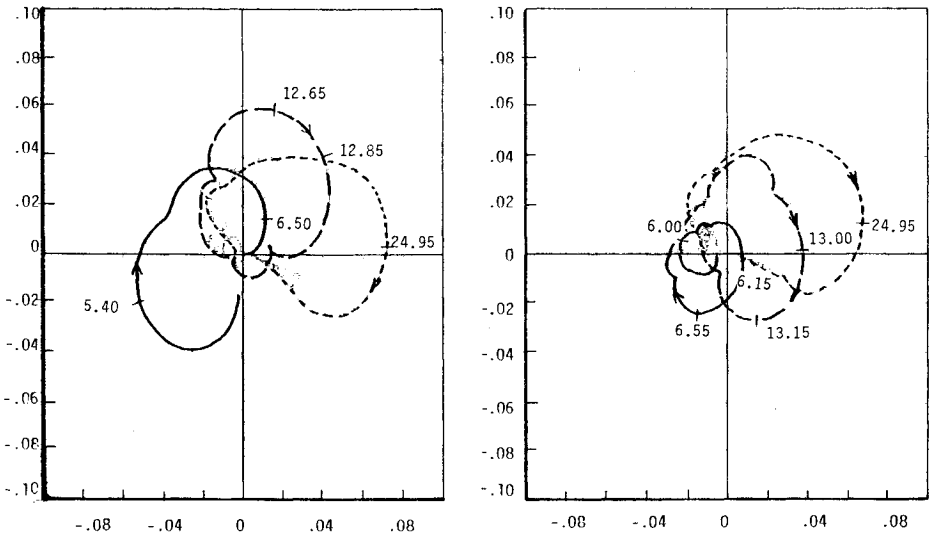

a) Control Law (N3). b) Control Law (N3P).

Fig. 17 Closed loop transfer functions $G_{11} = (a_3 - a_1)$ vs $\delta_{IN,LE}$.

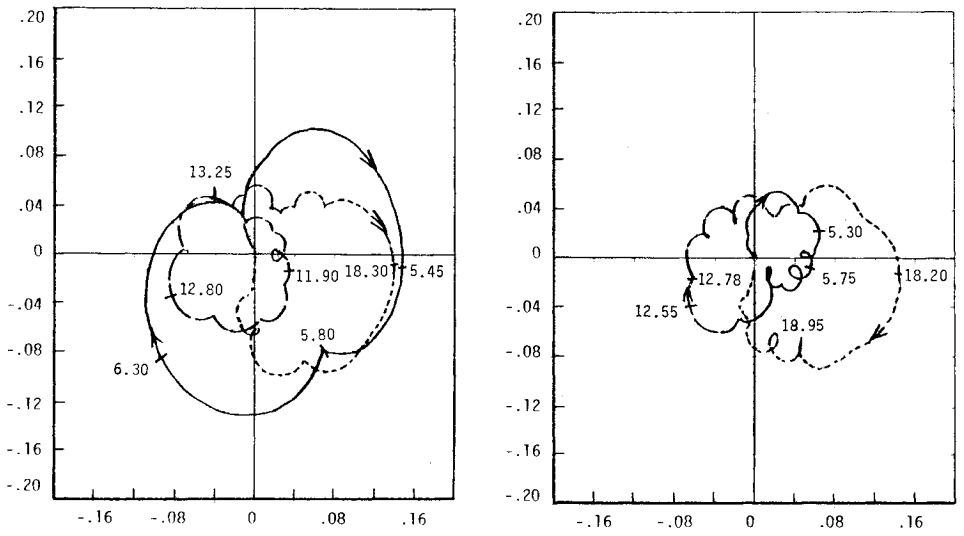

a) Control Law (N3T). b) Control Law (N3P).

Fig. 18 Closed loop transfer functions, $G_{22} = (a_4 - a_3)$ vs $\delta_{IN,TE}$.

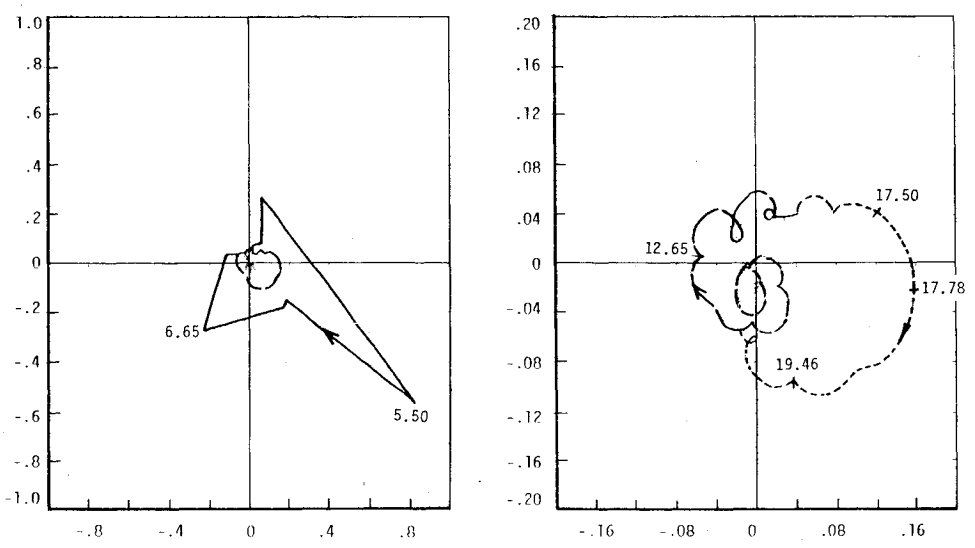

a) As computed. b) After eliminating the 6 Hz mode.

Fig. 19 Computed closed loop transfer function $G_{22,c}$ corresponding to control law (N3P).

Determination of System Frequencies and Dampings

The previous subsections describe how the measured transfer function data are prepared for identification of the system frequency and damping parameters. The HP Fourier Analyzer has a modal analysis package that is well suited for the identification task. One drawback of that system is that it cannot identify modes that are negatively damped. Hewlett Packard has provided Northrop with a modified version of the system that does have a capability for identifying unstable modes.

Another complicating factor in the identification process is that, near the flutter point, there are two lightly damped modes that are very close in frequency. This can confuse the identification system, with significant user interaction required to obtain satisfactory results. With these qualifications, Fig. 15 shows open loop frequency and damping estimates from the data gathered during Run No. 27 of the tunnel test. Only the two lowest frequency modes, which represent close to the total flutter mechanism, are shown. The dynamic pressure range is limited by the range over which it was prudent to excite the model. The flutter speed is 74 psf for this case with a strong crossing of the stability boundary.

Figure 16 also compares the open loop result with those obtained when control law (N3) was used (see Table 1). It is seen that, over the range measured, the system remains stable and in fact it is impossible to project a closed loop flutter speed. The comparison of the open and closed loop frequencies shows that the modes remain well separated when the control law is in force.

Finally, Fig. 16 shows the results of the two-surface control law, designated the (N3P) law. This law gives the best stability characteristics. In fact, the modal damping is so high that identification is considerably less precise for this case.

Additional Evaluation of the Control Laws

As described previously, control law (N3) is a leading edge surface law that uses transducer outputs (a_3-a_1) and (a_4-a_3) as the feedback signals. It was tested up to $(Q/Q_f)=1.70$. According to the peak-hold damping trend, this law has a potential to be effective up to $(Q/Q_f)=2.31$. On the other hand, control law (N3T) is a trailing edge surface law. This law also uses accelerometer outputs (a_3-a_1) and (a_4-a_3) as the feedback signals. Control law (N3T) was less effective than control law (N3). By combining the two control laws, a two-surface control law (N3P) was organized. Analysis, which was subsequently proven in the wind tunnel test, indicated the (N3P) law was an effective law. The block diagram of the two-surface law (N3P) is shown in Fig. 4. In the figure, $G_{11}...G_{22}$ are the open loop aircraft transfer functions due to the servo input to the control surfaces. $\bar{F}_1,\bar{F}_2$ are the feedback loops for the leading edge surface. They are identical to those used by control law (N3). $\bar{F}_3,\bar{F}_4$ are the feedback loops for the trailing edge surface. They are identical to those of control law (N3T).

In this section, closed loop transfer functions of the three control laws are presented side by side for a constant Q (80 psf) to show their relative effectiveness (Figs. 17 and 18).

Figure 17a is the closed loop transfer function of (a_3-a_1) vs the leading edge excitation $\delta_{\text{IN,LE}}$, when control law (N3) is active. The same transfer function corresponding to the two surface control law (N3P) at the same dynamic pressure is shown in Fig. 17b. In these plots, the numbers next to the curves refer to the frequency in Hertz. In comparing the two sets of transfer function data, and similar data for (a_4-a_3), general similarities are noted as to the major response modes, their frequencies and relative phasings to the excitation. For both (a_3-a_1) and (a_4-a_3), the response near the flutter frequency is substantially less for control law (N3P), indicating the law is more effective than the leading edge surface law (N3). For the trailing edge surface control law (N3T), the transfer function (a_4-a_3) due to $\delta_{\text{IN,TE}}$ is presented in Fig. 18a. The corresponding plot for the two-surface law (N3P) is shown in Fig. 18b. In comparing these plots, as well as those for (a_3-a_1), the general similarities between the two sets of transfer functions are again observed. Law (N3T) seems to be effective in suppressing the (a_3-a_1) response, a signal dominated by wing bending. On the other hand, (N3T) is much less effective than (N3P) in suppressing the (a_4-a_3) response, a signal dominated by wing torsion.

The open loop transfer functions $G_{11}...G_{22}$ of the model are extracted from the measured closed loop transfer functions for the single surface control laws (N3), (N3T). Assuming that the unsteady aerodynamic coefficients are linear, and that there is no or minimum interaction between the leading edge and trailing edge surfaces, the closed loop transfer functions of the two-surface law (N3P) are analytically generated using the open loop transfer function $G_{11}...G_{22}$ and the following formulas:

$$G_{11,c}=[(1+\bar{F}_2G_{21}+\bar{F}_4G_{22})G_{11}-(\bar{F}_2G_{11}+\bar{F}_4G_{12})G_{21}]/$$

$$[(1+\bar{F}_1G_{11}+\bar{F}_3G_{12})(1+\bar{F}_2G_{21}+\bar{F}_4G_{22})$$

$$-(\bar{F}_1G_{21}+\bar{F}_3G_{22})(\bar{F}_2G_{11}+\bar{F}_4G_{12})] \quad (3)$$

$$\cdots\cdots\cdots\cdots\cdots$$

$$G_{22,c}=[(1+\bar{F}_1G_{11}+\bar{F}_3G_{12})G_{22}-(\bar{F}_1G_{21}+\bar{F}_3G_{22})G_{12}]/$$

$$[(1+\bar{F}_1G_{11}+\bar{F}_3G_{12})(1+\bar{F}_2G_{21}+\bar{F}_4G_{22})$$

$$-(\bar{F}_1G_{21}+\bar{F}_3G_{22})(\bar{F}_2G_{11}+\bar{F}_4G_{12})] \quad (4)$$

Using Eqs. (3) and (4) the closed loop transfer functions for the two-surface control law (N3P) are computed. Typical data are shown in Fig. 19.

Both the numerators and the denominators of Eqs. (3) and (4) feature a sharp and narrow peak at the flutter frequency (6 Hz). Because of these peaks, and the lack of resolution in their neighborhood, large errors can be expected for $G_{11,c}$ and $G_{22,c}$ near the flutter frequency. This was indeed the case, as can be seen from the computed result of Fig. 19a. A comparison of the plot with the measured closed loop transfer function (Fig. 18b) indicates that there exist large differences in the amplitude of the polar curves representing the flutter mode, yet the phasings of the two sets of data are comparable.

When the major loop representing the flutter mode transfer functions is eliminated from the computed $G_{22,c}$ data, the transfer function shown in Fig. 19b results. The result may again be compared with the appropriate portion of the measured data of Fig. 18b. An examination of the plots shows that a close similarity does exist. This observation bears out the fact that, in the frequency range under consideration, the two-surface aerodynamic intercoupling is moderate.

Conclusions

Aircraft active wing/store flutter suppression has drawn substantial interest in the technical community dealing with aeroelastic problems. In concentrating on one severe flutter condition of the YF-17 model, it was possible to organize a number of control laws and test them in one tunnel entry. The wind tunnel test demonstrated a number of milestones which are listed below:

1) For three control laws, the model was tested at $Q/Q_f=1.70$, indicating a flutter speed improvement of approximately 30%. For control law (N3), a peak-hold damping prediction indicated a potential to reach a dynamic pressure 131% above the open loop flutter dynamic pressure;

2) The ability to switch from one control law to another at $Q/Q_f = 1.40$ was demonstrated. This feature is significant in future adaptive flutter control, where control law changes at supercritical speeds are necessary;

3) The ability to switch from a leading edge control law to a trailing edge control law, and vice versa, was also demonstrated;

4) Test monitoring programs were developed to closely monitor the flutter control system behavior in the wind tunnel.

The consistent performance of the active flutter suppression systems reinforces our confidence in the approach. Another technical step ahead involves the development of adaptive control laws for flutter suppression. The adaptive system is needed to deal with the varying wing/store configurations, or flight conditions, or both. With the advancement in digital computers and integrated aircraft control system, and through the concerted effort of the technical community, it is our feeling that working flutter suppression systems will eventually be incorporated in modern combat aircraft.

Acknowledgments

The work reported in this paper was conducted under AFFDL Contract F33615-78-C-3221, Additional Demonstration of Active Wing/Store Flutter Suppression Systems. The Air Force project engineer was Mr. Thomas E. Noll. The test engineer at the NASA Langley Center TDT facility was Mr. Moses G. Farmer. Other than the authors, key participants from Northrop include Messrs. George Mills, Don Patton, and Dr. Richard Tye.

References

[1]Hwang, C., Winther, B.A., Noll, T.E., and Farmer, M.G., "Demonstration of Aircraft Wing/Store Flutter Suppression Systems," AGARD Rept. R-668, July 1978.

[2]Hwang, C., Winther, B.A., and Mills, G.R., "Demonstration of Active Wing/Store Flutter Suppression Systems," AFFDL Rept. TR-78-65, June 1978.

[3]Johnson, E.H., "Flutter Control Law Definition Via Least Square Synthesis," *Proceedings of AIAA 21st Structures, Structural Dynamics and Materials Conference, Seattle, Wash., May 1980, pp. 595-603.*